Journal of Materials Chemistry A

Na2Ru1-xMnxO3 as the Cathodes for Sodium-Ion Batteries

Journal:	*Journal of Materials Chemistry A*
Manuscript ID	TA-COM-12-2018-011915.R1
Article Type:	Communication
Date Submitted by the Author:	30-Jan-2019
Complete List of Authors:	Li, Xiang; AIST, Guo, Shaohua ; NJU, College of Engineering and Applied Science Qiu, Feilong; Nanjing University Wang, Linlin; Nanjing University Ishida, Masayoshi; University of Tsukuba, Graduate School of Systems and Information Engineering Zhou, HaoShen; AIST, ; Nanjing university, Center of Energy Storage Materials & Technology

Journal Name

COMMUNICATION

$Na_2Ru_{1-x}Mn_xO_3$ as the Cathodes for Sodium-Ion Batteries

Xiang Li,[a, b, c] Shaohua Guo,[a, c]* Feilong Qiu, [a] Linlin Wang,[d] Masayoshi Ishida[b] and Haoshen Zhou[a, b, c]*

Received 00th January 20xx,
Accepted 00th January 20xx

DOI: 10.1039/x0xx00000x

www.rsc.org/

Sodium-ion batteries (SIBs) have attracted a surge of attention as the potential alternative replacing lithium-ion batteries (LIBs). However, the current cathodes of SIBs suffer from problems of limited capacity, capacity decay, inferior cycling performance and structural instability. Na_2RuO_3 is known for the high capacity including both cationic redox and anionic redox processes. Here we show a general method for improving the sodium storage performance of Na_2RuO_3 via Mn doping. A series of $Na_2Ru_{1-x}Mn_xO_3$ are explored through X-ray diffraction (XRD), galvanostatic charge-discharge test, electrochemical impedance spectroscopy (EIS) measurements and so on. The results exhibit that a suitable Mn doping (x=0.1) enhances the kinetics and structural stability of the electrode, accounting for a superior electrochemical performance. Our findings pave a simple method to develop the advanced cathodes for SIBs with a long lifespan and large capacity.

Increasing attention has been paid on the development of SIBs recently.[1-5] SIBs are regarded as the potential substitutes of LIBs due to the similar electrochemical properties between sodium and lithium and the abundant reserves of sodium compared with lithium. The layered $LiCoO_2$ cathode has been firstly commercialized by Sony Corporation.[6] It acquired a huge success and the Li-family cathodes have remained active in our daily lives. The successful experiences in LIBs can be introduced to design the high-power storage materials for SIBs. The layered Na_xTMO_2 (TM=transition metal) are considered to be the most promising cathodes.[7-18] However, they suffer from severe capacity decay mainly caused by the undesired phase transition stemming from the large size of sodium.[19-21] Thus, the structural stability is an important issue for developing large capacity and high reversible cathodes.

There is one type cathode of LIBs possessing the large capacity, which is called Li-rich layered cathode. Compared with other typical cathodes including sole cationic redox process during cycling for charge compensation, Li-rich layered cathode presents both cationic and anionic processes during cycling, which therefore delivers more lithium ions and then the high capacity. The oxygen in the lattice of Li-rich layered cathodes will be oxidized from O^{2-} to a higher valence of O^{n-} ($0 \le n < 2$). Tarascon *et al.* firstly observed the forming of O_2^{2-} by means of scanning transmission electron microscopy (STEM), presenting a better understanding of oxygen behaviour.[22] Our previous work also confirmed the O^{-1}-O^{-1} bonds forming mainly along the *c* axis directly by in-situ Raman and in-situ XRD, enriching the evidence of the anionic redox behaviour in Li-rich layered cathodes.[23] There are many cathodes reported based on this creative notion, such as Li_3IrO_4 and Li_3NbO_4-based system.[24-28] The successful experience in Li-rich cathodes can be reasonably ported to sodium-rich cathodes. Our group reported a sodium-rich layered material Na_3RuO_4 as the cathode with reversible anionic redox process.[29] Yamada *et al.* utilized Na_2RuO_3 as the cathode of SIBs.[30, 31] Na_2RuO_3 is a typical sodium-rich cathode which can be written as $Na(Na_{1/3}Ru_{2/3})O_2$ with $[NaRu_2]$ arrays in transition metal layers. The format of Na_2RuO_3 is similar to Li_2MnO_3, the electrochemical process, however, is different.[32, 33] Mn, with the valence of 4+, cannot be oxidized further during charging.[34] While Ru can be oxidized from 4+ to 5+. Yamada *et al.* confirmed there are both cationic redox (Ru^{4+}) and anionic redox (O^{2-}) processes in Na_2RuO_3. Tarascon *et al.* reported Sn^{4+}-doped Na_2RuO_3 compounds.[35] Song *et al.* studied $Na_2Ru_{0.95}Zr_{0.05}O_3$ by substitution of Zr for Ru.[36] The materials show electrochemical activity benefiting from the high electronic conductively of Ru and special Na-rich structure. However, the improvement of electrochemical performance for these doped cathodes is not pronounced.

Herein, we apply Mn-doped Na_2RuO_3 as the cathodes of SIBs and explore the influence of different content Mn on Na_2RuO_3. The results show that an appropriate Mn doping can elevate the kinetics and structural stability of Na_2RuO_3, promoting the electrochemical performance. The facile method opens the

[a] *Center of Energy Storage Materials & Technology, College of Engineering and Applied Sciences, National Laboratory of Solid State Microstructures, and Collaborative Innovation Center of Advanced Microstructure, Jiangsu Key Laboratory of Artificial Functional Materials, Nanjing University, Nanjing 210093, China. *Email: shguo@nju.edu.cn, hszhou@nju.edu.cn.*

[b] *Division of Engineering Mechanics and Energy, Faculty of Engineering, Information and Systems, University of Tsukuba, Tennoudai 1-1-1, Tsukuba, 305-8573, Japan.*

[c] *Energy Technology Research Institute, National Institute of Advanced Industrial Science and Technology (AIST), Japan.*

[d] *Nanjing Univ, Sch Chem & Chem Engn, Collaborat Innovat Ctr Chem Life Sci, State Key Lab Analyt Chem Life Sci, Nanjing 210093, Jiangsu, Peoples R China*

† Electronic Supplementary Information (ESI) available. See DOI: 10.1039/x0xx00000x

way to design the Na-rich layered materials with large capacity and long-life cycling stability.

The XRD patterns of the series $Na_2Ru_{1-x}Mn_xO_3$ (x = 0, 0.1, 0.3, 0.5, 0.7 and 1) are firstly displayed in **Figure 1**. The simulated standard Na_2RuO_3 and Na_2MnO_3 pattern are also shown for comparing. The peaks of Na_2RuO_3 can be indexed well with O3 type structure (space group: R-3m) defined by Delmas with undetectable superlattice peaks locating from ~ 20° to 30°.[37] It is clear that when x value is larger than 0.3, there is one additional peak appearing near 16° (more obvious in **Figure 1b**), indicating the material contains two phases. This peak grows up with the increasing x value, meanwhile, the (003) peak of O3 type decreases progressively. The additional phase coincides with Na_2MnO_3 phase (space group: C2/m) meaning that the Na_2MnO_3-type structure dominates the whole structure when x value is large. The heterogeneous system may result from the large radii difference between Mn^{4+} (0.53 Å) and Ru^{4+} (0.62 Å).[38] However, the material also shows a single phase when the x value is lower than 0.3, consistent well with the layered O3 type structure. The Mn/Ru distribution should be not ordered because there is no evidence of superlattice peaks.[30] The SEM (scanning electron microscope) images also display the difference between these materials, as shown in Figure 1c-1h. The morphology of sample x = 0 is irregular. When x increases to 0.1, the particles present uniform and regular layered blocks, indicating a homogeneous phase. However, there appear some small particles on the layered blocks when x changes to 0.3, implying that there exists impurity in the sample. More obvious phenomena are captured when x is larger than 0.3. The morphologies are similar for the sample x = 0.5, 0.7, and 1, containing the predominant small particles affixing on the big blocks. To further confirm the difference of $Na_2Ru_{1-x}Mn_xO_3$, transmission electron microscope (TEM) was performed. The results are shown in **Figure S1**. Similar with SEM results, the samples when x < 0.3 show clear layered structure highlighted by the yellow rectangle, especially the sample x = 0.1. The sample x = 0.3 emerges more than one phase evidenced by the inserted selected area electron-diffraction pattern. When x > 0.3, the TEM images show another crystal lattice marked by the pink rectangle. The results are consistent well with that of SEM and XRD.

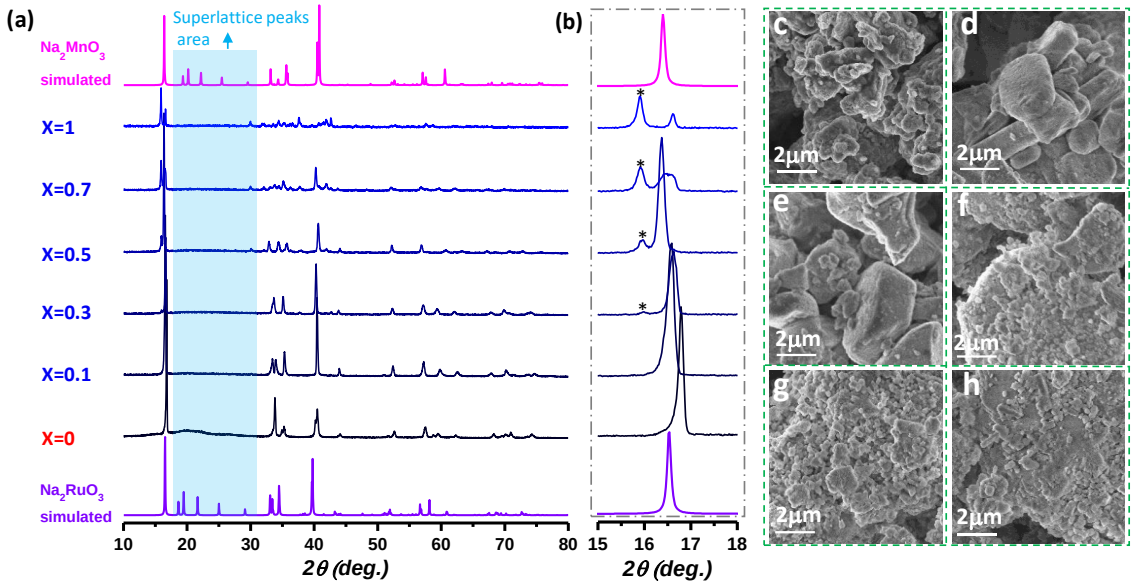

Figure 1. (a) XRD patterns of $Na_2Ru_{1-x}Mn_xO_3$ with simulated Na_2RuO_3 and Na_2MnO_3. (b) XRD patterns of (a) with an enlarged scope of 2θ from 15° to 18°. The SEM images of $Na_2Ru_{1-x}Mn_xO_3$ for (c) x = 0, (d) x = 0.1, (e) x = 0.3, (f) x = 0.5, (g) x = 0.7, and (h) x = 1.

The typical galvanostatic potential curves of $Na_2Ru_{1-x}Mn_xO_3$ are shown in **Figure 2a**, with the initial two cycles at the current density of 10 mA g^{-1}. The x value is 0, 0.1, 0.3, 0.5 and 0.7 from bottom to up. There are three key points should be noticed. The first is capacity. For the theoretical capacity of traditional cathodes, it is calculated by the cationic redox process (Ru^{4+}/Ru^{5+} for here). The theoretical capacity is assigned by the green area in **Figure 2a** and the maximum capacity is decided by the number of sodium-ions which is labelled by the red dot line. For the overview, the capacity increases regularly with the increase of x value. Note that the content of Ru decreases when the x value increases, which means the theoretical capacity based on Ru redox decreases, as shown in the gradient green area. Synchronously, the capacity beyond the theoretical value, where the additional one belongs to the oxygen redox, increases with the increasing x value. For the sample x = 0.5, the capacity is larger than the maximum value, which is ascribed to the electrolyte decomposition. The second is the plateau of the oxygen redox reaction. Li-rich layered materials have a significant symbol of a ~ 4.5 V long plateau attributing to the oxygen redox in the first cycle which is different from subsequent cycles.[39-42] For the series of $Na_2Ru_{1-x}Mn_xO_3$, this plateau is located at ~ 4.0 V and the plateau prolongs when x value increases, demonstrating the Mn-doped Na_2RuO_3 can activate the oxygen behaviour. The higher content of Mn is, the higher capacity

releases when we focus on the first charge process. The reversibility of the capacity is an important factor we concern, which is the key point three. **Figure 2a** displays the irreversible sodium ions compared the first charge and discharge processes. The irreversible values are 0.22, 0.41, 0.43, 1.25 and 1.01 for the sample x = 0, 0.1, 0.3, 0.5 and 0.7, respectively. The sample x = 0 shows the best reversibility during the first cycle. And the reversibility deteriorates with the increasing content of Mn, especially when x value is higher than 0.5. To explore the reason influencing the capacity reversibility, dQ/dV curves are performed in **Figure 2b**. The samples exhibit the analogous curves in the first cycle, thus we focus on the second cycle and their derivate dQ/dV curves. The apparent difference in **Figure 2b** is highlighted by the dot black rectangle. There are some peaks locate beyond 3.5 V when x is larger than 0.1, indicating the phase transitions in these materials.[43-45] The undesired phase transitions deteriorate the structural stability and aggravate the failure of the capacity eventually. For comparison, there are no peaks above 3.5 V for the sample x = 0 and 0.1, evidencing that there is no phase transition at high potential. Especially, the galvanostatic potential curves of sample Na_2MnO_3 (x = 1) are shown in **Figure S2**. The charge capacity is only ~ 30 mAh g^{-1}, corresponding to 0.17 Na^+ per formula, far less than 2 Na^+ in the formula. There are many peaks in dQ/dV curves, indicating the Mn redox process and undesired phase transitions. Additionally, the dQ/dV curves of the first cycle for $Na_2Ru_{1-x}Mn_xO_3$ are shown in **Figure S3**. Note that the XRD of Na_2MnO_3 is not coincided well with the simulated Na_2MnO_3, demonstrating that the phase of Na_2MnO_3 is unstable and impure. It is intelligible that the structure of $Na_2Ru_{1-x}Mn_xO_3$ would be unstable when x increased, corresponding to the phase separation in **Figure 1** and phase transitions in **Figure 2b**. The comparison of different $Na_2Ru_{1-x}Mn_xO_3$ with charge capacity, discharge capacity and coulombic efficiency for the first cycle are shown in **Figure S4**. The gap between charge and discharge capacity expands with x increases (except x = 1), representing the irreversibility. The electrochemical performance of the samples x = 0 and 0.1 are better than others apparently.

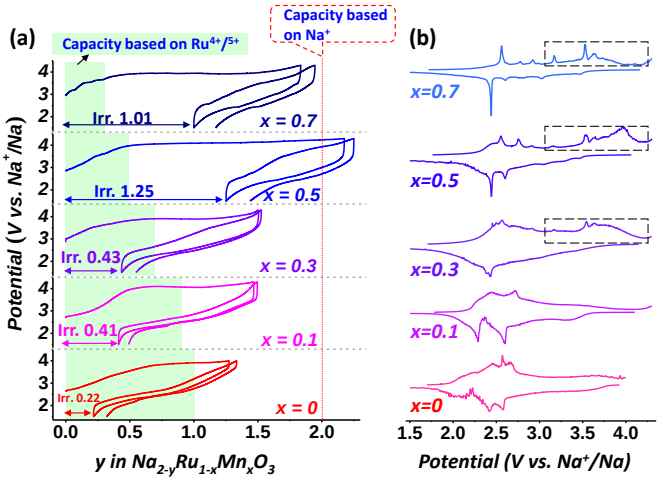

Figure 2. (a) The typical galvanostatic potential curves of $Na_2Ru_{1-x}Mn_xO_3$ for the initial two cycles at the current density of 10 mA g^{-1}. The potential window is from 1.5 V to 4 V for sample x = 0 and from 1.5 V to 4.3 V for other samples. (b) The corresponding dQ/dV curves with the second cycle derived from (a).

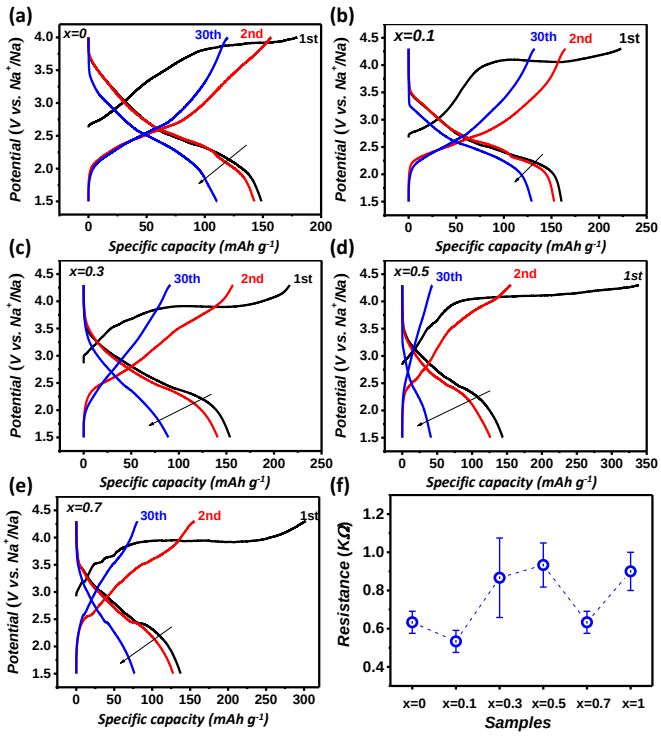

Figure 3. Electrochemical performance of $Na_2Ru_{1-x}Mn_xO_3$. Typical galvanostatic charge-discharge profiles of (a) x=0, (b) x=0.1, (c) x=0.3, (d) x=0.5 and (e) x=0.7. The current density is 20 mA g^{-1}. (f) The resistances of different cathodes of $Na_2Ru_{1-x}Mn_xO_3$ by using 4-point conductivity with error bar.

To deeply compare the electrochemical performance of $Na_2Ru_{1-x}Mn_xO_3$, the galvanostatic profiles at the current density of 20 mA g^{-1} are exhibited for the initial 30 cycles in **Figure 3**. The electrodes deliver the discharge capacity of 110.2, 130.4, 88.8, 41.1, and 76.7 mAh g^{-1} at the 30th cycle for the sample x = 0, 0.1, 0.3, 0.5 and 0.7 respectively. The corresponding capacity retention after 30 cycles

are 74.0%, 81.0%, 57.7%, 28.6%, and 55.8%, respectively. The sample x = 0.1 displays the largest capacity and highest capacity retention at a low current density, followed by the sample x = 0. For the high Mn content ($x \geq 0.3$) samples, the structures are unstable and suffer from the undesired and severe phase transitions, resulting in inferior capacity performance. The cycling curves of $Na_2Ru_{1-x}Mn_xO_3$ for the initial 30 cycles are shown in **Figure S5**. The changing trend of discharge capacity for the sample x = 0.1 is gentle with a flat gradient. However, the samples with high Mn content exhibit serious degrade. The sample x = 0.1 exhibits the best electrochemical performance of all samples. To further investigate the difference between the sample x = 0.1 and other samples, the resistances of different cathodes were tested by using 4-point conductivity. The results are shown in **Table S6** and **Figure 3f**. The resistance of sample x = 0.1 is smaller than others, indicating the great improvement of conductivity. Additionally, EIS curves of $Na_2Ru_{1-x}Mn_xO_3$ for the pristine half-cells and the cells after 100 cycles at the current density of 100 mA g^{-1} with suitable fitting are also shown in **Figure S7**, further indicating the superior kinetics when doping suitable Mn.

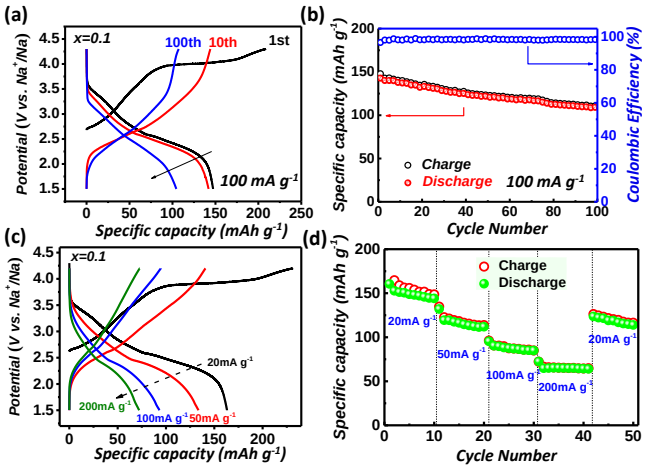

Figure 4. Electrochemical performance of $Na_2Ru_{0.9}Mn_{0.1}O_3$. (a) Typical galvanostatic charge-discharge profiles at the current density of 100 mA g^{-1}. (b) The cycling performance for the sample x = 0.1 at the current density of 100 mA g^{-1}. (c) The galvanostatic charge-discharge profiles at the different densities of 20, 50, 100 and 200 mA g^{-1}. (d) The rates performance at the different current densities.

In view of the best behaviour shown in the sample x = 0.1, we continue to focus on its cycling performance at high current density, the results are shown in **Figure 4**. The sample displays a capacity of 108.1 mAh g^{-1} after 100 cycles at the current density of 100 mA g^{-1}, presenting a capacity retention of 75.72% and a stable coulombic efficiency of ~ 97.7%. The rates performance was obtained at different current densities of 20, 50, 100 and 200 mA g^{-1} respectively for every 10 cycles. The corresponding capacities for the first cycle at every current density are 160.4, 105.8, 77.3 and 57.3 mAh g^{-1}, respectively (the corresponding normalized curves of discharge capacity are shown in **Figure S8** for comparison). The capacity recovers to a high level of 112.6 mAh g^{-1} after returning the current density from 200 mA g^{-1} back to 20 mA g^{-1}, demonstrating the good structural stability of the sample. Further, ex-situ XRD pattern of sample x = 0.1 after 100 cycles at the current density of 100 mA g^{-1} is revealed, as shown in **Figure S9**. The corresponding pattern of Na_2RuO_3 is also uncovered for comparison. The peaks of cycled Na_2RuO_3 degrade severely, indicating a shift of structure from crystalline to amorphous, which is related to the performance decay. There also exists phase transition from O3 structure of pristine to O3+P3 mixed structure of the cycled electrode, evidenced by the split of (003) peak. For the sample x = 0.1, the changing trend is analogous to that of Na_2RuO_3. However, the peaks maintain tough and the structure preserves well crystallinity. Both the high kinetics during cycles and good crystallinity accounts for a favorable electrochemical performance of the sample x = 0.1. Furthermore, the comparison among Mn-doped, Zr-doped, and Sn-doped Na_2RuO_3 are displayed in **Table S10**, demonstrating a superior improvement by Mn-doping.

Conclusions

In summary, a series of Mn-doped Na_2RuO_3 with different concentration are investigated as cathodes for SIBs. A suitable Mn-doped Na_2RuO_3 (x = 0.1) has a positive effect on the electrochemical performance. The charge capacity of the first cycle is prolonged obviously with increased Mn content. However, the high content of Mn attenuates the structural stability of the sample, companied by undesired phase transitions at high potential and evident capacity fade. The sample x = 0.1 exhibits the best capacity retention of 81.0% after 30 cycles at 20 mA g^{-1} and delivers the highest capacity of 108.1 mAh g^{-1} after 100 cycles at 100 mA g^{-1}. The 4-point conductivity, EIS and ex-situ XRD results disclose that a suitable Mn amount enhances the kinetics and good crystallinity of the electrode, accounting for a better electrochemical performance. Our findings pave a simple method to improve the performance of Na_2RuO_3, promoting the development of Na-rich layered electrodes for SIBs with a long lifespan and large capacity in the future.

Acknowledgment

X. Li is grateful for the financial support of the CSC (China Scholarship Council) scholarship. This work was partially supported financially by National Basic Research Program of China (2014CB932300), NSF of China (21633003, 51802149, 11704245, and 11874199) and NSF of Jiangsu Province, China (BK20170630). We are very grateful to Dr Yijie Liu for the discussion.

Notes and references

The authors declare no competing financial interests.

1. N. Yabuuchi, K. Kubota, M. Dahbi and S. Komaba, *Chem. Rev.*, 2014, 114, 11636.
2. C. Zhao, Q. Wang, Y. Lu, B. Li, L. Chen and Y. S. Hu, *Sci. Bull.*, 2018, 63, 1125.

3. M. Li, N. Feng, M. Liu, Z. Cong, J. Sun, C. Du, Q. Liu, X. Pu and W. Hu, *Sci. Bull.*, 2018, 63, 982.
4. L. P. Wang, L. Yu, X. Wang, M. Srinivasan and Z. J. Xu, *J. Mater. Chem. A*, 2015, 3, 9353.
5. J. Y. Hwang, S. T. Myung and Y. K. Sun, Chem. *Soc. Rev.*, 2017, 46, 3529.
6. T. Nagaura, *Prog. Batteries Sol. Cells*, 1990, 9, 209.
7. N. Yabuuchi, M. Kajiyama, J. Iwatate, H. Nishikawa, S. Hitomi, R. Okuyama, R. Usui, Y. Yamada and S. Komaba, *Nat. Mater.*, 2012, 11, 512.
8. S. Guo, Q. Li, P. Liu, M. Chen and H. Zhou, *Nat. Commun.*, 2017, 8, 135.
9. S. Guo, P. Liu, Y. Sun, K. Zhu, J. Yi, M. Chen, M. Ishida and H. Zhou, *Angew. Chem. Int. Ed.*, 2015, 54, 11701.
10. S. Guo, Y. Sun, P. Liu, J. Yi, P. He, X. Zhang, Y. Zhu, R. Senga, K. Suenaga and M. Chen, *Sci. Bull.*, 2018, 63, 376.
11. Q. Li, Y. Qiao, S. Guo, K. Jiang, Q. Li, J. Wu and H. Zhou, *Joule*, 2018, 2, 1134.
12. D. Yuan, W. He, F. Pei, F. Wu, Y. Wu, J. Qian, Y. Cao, X. Ai and H. Yang, *J. Mater. Chem. A*, 2013, 1, 3895.
13. J. E. Wang, W. H. Han, K. J. Chang, Y. H. Jung and D. K. Kim, *J. Mater. Chem. A*, 2018, 6, 22731.
14. X. Chen, X. Zhou, M. Hu, J. Liang, D. Wu, J. Wei and Z. Zhou, *J. Mater. Chem. A*, 2015, 3, 20708.
15. L. Vitoux, M. Guignard, J. Darriet and C. Delmas, *J. Mater. Chem. A*, 2018, 6, 14651.
16. S. Guo and H. Zhou, *Science Bulletin*, 2019, DOI: 10.1016/j.scib.2019.01.004.
17. D. Yuan, X. Hu, J. Qian, F. Pei, F. Wu, R. Mao, X. Ai, H. Yang and Y. Cao, *Electrochim. Acta*, 2014, 116, 300.
18. D. Yuan, X. Liang, L. Wu, Y. Cao, X. Ai, J. Feng and H. Yang, *Adv. Mater.*, 2014, 26, 6301.
19. P. K. Nayak, L. Yang, W. Brehm and P. Adelhelm, *Angew. Chem. Int. Ed.*, 2018, 57, 102.
20. Y. Wang, D. Yuan, Z. Chen, J. Qian, X. Ai, Y. Cao and H. Yang, *Electrochim. Acta*, 2016, 222, 862.
21. Z. Yi, Z. Wang, Y. Cheng and L. Wang, *Energy Environ. Adv.*, 2018, 1, 132.
22. E. McCalla, A. M. Abakumov, M. Saubanere, D. Foix, E. J. Berg, G. Rousse, M. L. Doublet, D. Gonbeau, P. Novak, G. Van Tendeloo, R. Dominko and J. M. Tarascon, *Science*, 2015, 350, 1516.
23. X. Li, Y. Qiao, S. Guo, Z. Xu, H. Zhu, X. Zhang, Y. Yuan, P. He, M. Ishida and H. Zhou, *Adv. Mater.*, 2018, 30, 1705197.
24. Q. Jacquet, A. Iadecola, M. Saubanère, L. Lemarquis, E. J. Berg, D. Alves Dalla Corte, G. Rousse, M. L. Doublet and J. M. Tarascon, *Chem. Mater.*, 2018, 30, 7682.
25. Q. Jacquet, A. Perez, D. Batuk, G. Van Tendeloo, G. Rousse and J. M. Tarascon, *Chem. Mater.*, 2017, 29, 5331.
26. A. J. Perez, Q. Jacquet, D. Batuk, A. Iadecola, M. Saubanère, G. Rousse, D. Larcher, H. Vezin, M. L. Doublet and J. M. Tarascon, *Nat. Energy*, 2017, 2, 954.
27. W. H. Kan, D. Chen, J. K. Papp, A. K. Shukla, A. Huq, C. M. Brown, B. D. McCloskey and G. Chen, *Chem. Mater.*, 2018, 30, 1655.
28. N. Yabuuchi, M. Takeuchi, M. Nakayama, H. Shiiba, M. Ogawa, K. Nakayama, T. Ohta, D. Endo, T. Ozaki and T. Inamasu, *Proc. Natl. Acad. Sci.,* 2015, 112, 7650.
29. Y. Qiao, S. Guo, K. Zhu, P. Liu, X. Li, K. Jiang, C. J. Sun, M. Chen and H. Zhou, Energy Environ. Sci., 2018, 11, 299.
30. B. M. De Boisse, G. Liu, J. Ma, S.-i. Nishimura, S. C. Chung, H. Kiuchi, Y. Harada, J. Kikkawa, Y. Kobayashi and M. Okubo, *Nat. Commun.*, 2016, 7, 11397.
31. M. Tamaru, X. Wang, M. Okubo and A. Yamada, *Electrochem. Commun.*, 2013, 33, 23.
32. L. Zheng, H. Wang, M. Luo, G. Wang, Z. Wang and C. Ouyang, *Solid State Ionics*, 2018, 320, 210.
33. M. H. N. Assadi, M. Okubo, A. Yamada and Y. Tateyama, *J. Mater. Chem. A*, 2018, 6, 3747.
34. J. Roos, C. Eames, S. M. Wood, A. Whiteside and M. Saiful Islam, *Phys. Chem. Chem. Phys.*, 2015, 17, 22259.
35. P. Rozier, M. Sathiya, A. R. Paulraj, D. Foix, T. Desaunay, P. L. Taberna, P. Simon and J. M. Tarascon, *Electrochem. Commun.*, 2015, 53, 29.
36. S. Song, M. Kotobuki, F. Zheng, Q. Li, C. Xu, Y. Wang, W. D. Z. Li, N. Hu and L. Lu, *J. Power Sources*, 2017, 342, 685.
37. C. Delmas, C. Fouassier and P. Hagenmuller, *Physica B+ C*, 1980, 99, 81.
38. R. D. Shannon, *Acta Crystallogr., Sect. A*, 1976, 32, 751.
39. M. M. Thackeray, S. H. Kang, C. S. Johnson, J. T. Vaughey, R. Benedek and S. Hackney, *J. Mater. Chem.*, 2007, 17, 3112.
40. Z. Xiao, J. Meng, Q. Li, X. Wang, M. Huang, Z. Liu, C. Han and L. Mai, *Sci. Bull.*, 2018, 63, 46.
41. Y. Gao, J. Ma, X. Wang, X. Lu, Y. Bai, Z. Wang and L. Chen, *J. Mater. Chem. A*, 2014, 2, 4811.
42. K. Shimoda, T. Minato, K. Nakanishi, H. Komatsu, T. Matsunaga, H. Tanida, H. Arai, Y. Ukyo, Y. Uchimoto and Z. Ogumi, *J. Mater. Chem. A*, 2016, 4, 5909.
43. R. Berthelot, D. Carlier and C. Delmas, *Nat. Mater.*, 2010, 10, 74.
44. L. Vitoux, M. Guignard, M. R. Suchomel, J. C. Pramudita, N. Sharma and C. Delmas, *Chem. Mater.*, 2017, 29, 7243.
45. Z. Chen, Z. Lu and J. Dahn, *J. Electrochem. Soc.*, 2002, 149, A1604.